Materials Advances

Accepted Manuscript

This article can be cited before page numbers have been issued, to do this please use: A. K. Das, M. S. Ali, A. Misra, M. S. Saikh, S. Dhibar, S. K. Panja, A. Das, G. Ghatak, L. K. Rathore, A. Bera, S. Bhar and S. Biswas, *Mater. Adv.*, 2026, DOI: 10.1039/D5MA00879D.

ROYAL SOCIETY OF CHEMISTRY

rsc.li/materials-advances

Eco-friendly Cyanation Strategies of Aryl Halides using Recyclable Nickel Nanocatalysts with Promising Antibacterial and Antioxidant Activities

View Article Online
DOI: 10.1039/D5MA00879D

Asit Kumar Das,[a,*] Md Sattar Ali,[a] Arindam Misra,[a] Md Sultan Saikh,[a] Subhendu Dhibar,[b] Sumit Kumar Panja,[c] Aniruddha Das,[d] Gourav Ghatak,[e] Lokesh Kumar Rathore,[f] Ashok Bera,[f] Sanjay Bhar,[g] Smritikana Biswas,[e,*]

[a]Department of Chemistry, Murshidabad University, Berhampore, 742101, India.
E-mail: akdche@msduniv.ac.in
[b]Department of Physics, Indian Institute of Technology Patna, Bihar, 801106, India.
[c]Tarsadia Institute of Chemical Science, Uka Tarsadia University, Surat, 394350, India.
[d]Department of Chemistry, Shiv Nadar Institution of Eminence Deemed to be University, Uttar Pradesh, 201314, India.
[e]Department of Physiology, Murshidabad University, Berhampore, 742101, India.
E-mail: physio.smriti2005@gmail.com
[f]Department of Physics, Indian Institute of Technology Jammu, Jammu, J & K 181221, India.
[g]Department of Chemistry, Jadavpur University, Kolkata-700032, India.

ABSTRACT

Recyclable nickel nanoparticles have been utilized as an effficient, stable, heterogeneous catalyst for the synthesis of aryl nitriles using commercially available and less toxic $K_4[Fe(CN)_6].3H_2O$ as an environmentally benign cyanide source. The reactions are not dependent on an inert atmosphere or a ligand. Several aryl chlorides, aryl bromides and aryl iodides survived well and were associated with high yield in the aforesaid method. The synthesized Ni-γAl_2O_3 nanocatalysts could be recovered and recycled again without significantly reducing their efficacy. Moreover, "Sheldon's test (hot filtration method)" was carried out to establish the heterogeneity of the catalyst. The significant benefits of this catalytic methodology align with green chemistry principles, making this process potentially applicable in industrial chemistry. The synthesized Ni-γAl_2O_3 nanocatalysts exhibited moderate antioxidant activity, with maximum antioxidant activity (68.17%) found at 200 mg/ml concentration. Ni-γAl_2O_3 nanocatalysts were found to be effective against *Staphylococcus aureus* ATCC25923 (Gram-positive) and *Escherichia coli* (Gram-negative) with zones of inhibition of 10±0.25mm and 12±0 respectively. MIC values against

View Article Online
DOI: 10.1039/D5MA00879D

Escherichia coli (Gram-negative) and *Staphylococcus aureus* ATCC25923 (Gram-positive) were 200 mg/mL and 205 mg/mL respectively, while MBC values were 220 and 230 mg/mL for *Staphylococcus aureus* ATCC25923 and *Escherichia coli* respectively. This study is provided to afford the dual applicability of the recyclable Ni-γAl_2O_3 nanocatalyst for the green synthetic route of aryl nitriles and exhibiting potential antibacterial as well as antioxidant activity.

KEYWORDS: Cyanation, Nickel nanoparticles, Nitriles, Recyclable catalyst, Antibacterial activity.

1. INTRODUCTION

Nanomaterials have been appeared as one of the most emerging tools for biomedical as well as pharmaceutical applications.[1] It is necessary to stop the risk of pathogenic bacteria in terms of community health safety. Numerous types of antibacterial agents are being emerged. On the other hand, adverse effects and consecutive use of antibacterial agents lead to resistant towards antibiotics.[2-6] Concerning the recent trend in the substitute antimicrobial strategy, metal nanoparticles have promising dynamic and potential applications due to their unique as well as several chemical and physical properties.[2,7] Although, nickel nanoparticles (Ni NPs), a metal nanoparticle exhibits significant and effective antimicrobial property against several kinds of bacterial strain including pathogenic also.[8] Larger surface area, high reactivity of Ni NPs boosts and induces its antibacterial property (10 Bauer).

Aryl nitriles represent an important structural framework in the field of organic chemistry because of their multifarious application in diverse disciplines including polymers, materials, pharmaceuticals, agrochemicals, dyes, pigments, natural products, as well as biologically active compounds.[9] In addition, nitriles are straightforwardly converted into a range of several efficient scaffolds such as amidines, amides, oximes, aldehydes, ketones, esters and carboxylic acids.[10] Benzonitriles are the key intermediate in organic synthesis and used as industrially important solvent to carry out several significant organic transformations.[11] Furthermore, nitriles moieties are essential building blocks in pharmaceutically potential drugs, such as Letrozole®, Finrozole®, Citalopram®, Etravirine®, Periciazine®, Bicalutamide® and 5-lipoxygenase inhibitors have been recognised (Figure 1).[12] Historically, two conventional methods have been employed to synthesize aryl nitriles: diazotization of aromatic amines followed by a Sandmeyer reaction[13a-13d] and Rosenmund-von Braun reaction of aromatic halides.[13e] However, these reactions associated with serious disadvantages such

View Article Online
DOI: 10.1039/D5MA00879D

as high temperature, requirement of super-stoichiometric amount of extremely poisonous CuCN as cyanating agent and generation of major amount of heavy metal waste which leads to unavoidable environmental complications.

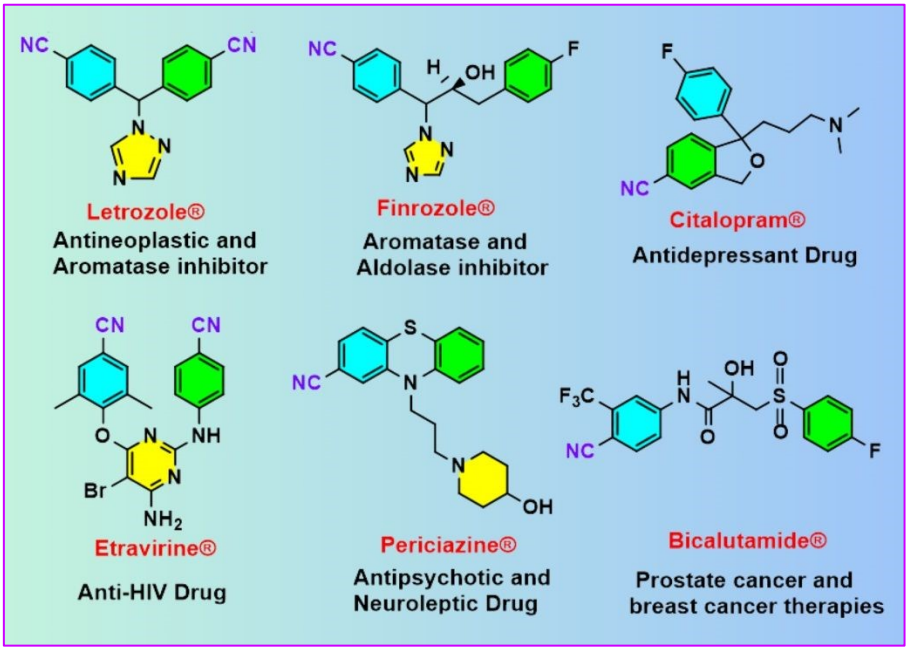

FIGURE 1 Some pharmaceutically potential organonitrile drugs

Therefore, the development of highly efficient and eco-friendly methodologies for the synthesis of important organic molecules is of significant importance.[14] In this context, the transition metal-mediated cyanation of aryl halides[15] for synthesizing the corresponding nitriles has gained immense attention from the scientific community. In 1973, Takagi *et al*. first developed the Pd catalyzed cyanation reaction of aryl bromides and aryl iodides using KCN as a cyanide source at 140-150^{o}C.[16] Later on, numerous transition metals, including Pd,[17a] Rh,[17b] Ir,[17c] and Cu[17d] were used in the synthesis of nitriles in the presence of toxic cyanating agents, such as $Zn(CN)_2$,[18a] CuCN,[18b] TMSCN,[18c] KCN,[18d] and NaCN.[17a,18e] Some less toxic nonmetallic agents such as aliphatic nitriles,[19a] cyanohydrins from acetone,[19b] benzyl thiocyanate,[19c] phenyl cyanate,[19d] and N-cyanobenzimidazole[19e] were also utilized with the employment of various hazardous and expensive nitrogen and phosphorus ligands. However, most of these protocols were highly poisonous both to humans as well as environment and caused high risk during handling and workup procedures which limited their industrial application. Therefore, the situation demanded the environmental benign chemical processes[20] for the syntheses of aryl nitriles using non-hazardous and economically safe cyanating agent. Beller and co-workers[17a] first reported the application of a commercially available eco-friendly $K_4[Fe(CN)_6]$ as a cyanating agent for the cyanation of aryl halides with

$Pd(OAc)_2$ as the metal precursor with dppf as the ligand. Recently, nickel-catalyzed[21] cyanation reactions (Scheme 1) have drawn significant attention due to their easy accessibility, lower toxicity, inexpensive and eco-friendly nature in comparison to the reported metal mediated reaction. Although the nickel catalysed developed procedures (Scheme 1) are quite acceptable, their limitations are significant because of the involvement of expensive cyanide sources, perilous ligands, laborious catalyst preparation, necessity of additives, generation of metal waste, recyclability problem of the catalysts, and difficult work-up methods that are less eco-friendly from the perspective of sustainability.[22]

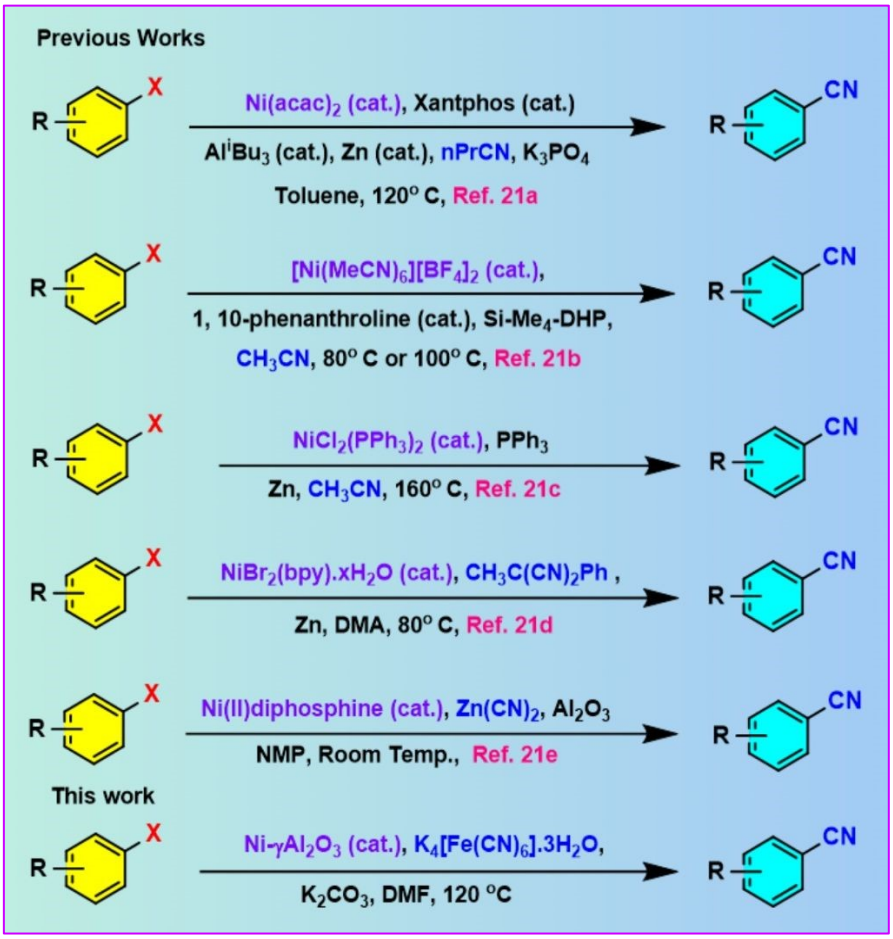

SCHEME 1 Ni catalysed different approaches for the cyanation of aryl halides

Therefore, considering the present environmental scenario, there is an enormous demand to develop highly effective approaches[23] for the synthesis of nitriles that refrain from utilizing expensive and harmful metal catalysts and rather employ less hazardous and less expensive reagents. However, in continuing on our previous work utilizing nickel nanocatalysts,[24] we have reported here the excellent catalytic attributes of Ni-γAl_2O_3 nanocatalyst (Scheme 1) for

View Article Online
DOI: 10.1039/D5MA00879D

the efficient synthesis of aryl nitriles from the cyanation reaction of aryl halides using innocuous $K_4[Fe(CN)_6].3H_2O$ as an eco-friendly cyanide source.

2. EXPERIMENTAL

2.1. Preparation of nickel nanocatalysts:

Nickel acetylacetonate (Merck), hydrazine hydrate (Sigma Aldrich), sodium hydroxide (Merck), PEG-400 (Loba Chemie) and ethanol (Merck) have been used as received. Every experiment was conducted using deionized water. The synthetic method includes dissolving 5 mmol of $Ni(acac)_2$ (nickel acetylacetonate) in 20 ml of PEG-400 solvent, and it was magnetically stirred for 20 minutes at room temperature. 2 ml of 0.1 M NaOH was then added, followed by the addition of 2 ml of hydrazine hydrate. Here, hydrazine hydrate serves as reducing agent and NaOH maintains the process alkaline in the reaction. By this time, the reaction mixture had changed color from green to deep blue. The reaction mixture was stirred magnetically at 80°C for 2 hrs and a black precipitate was obtained, which indicates the reduction of Ni^{2+} to Ni^0. Then, γ-Al_2O_3 (5 g) was added to the aforesaid mixture containing nickel nanoparticles and the reaction mixture was magnetically stirred for 1 hr. The reaction mixture was then allowed to cool to room temperature, washed successively with ethanol and water. The resultant residue was dried in an oven at 120ºC for 24h. Then it was stored under the ambient condition for its further investigation. Here, Figure 1 displays the schematic presentation used in this work for synthesizing heterogeneous nickel nanocatalysts.

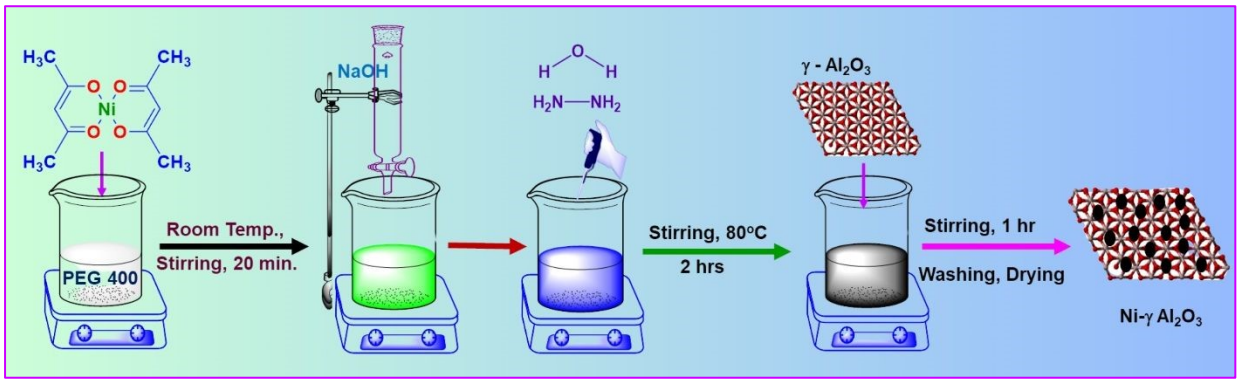

FIGURE 1 Schematic representation for the synthesis of Ni-γAl_2O_3 nanocatalyst.

2.2. Ni-γAl_2O_3 catalysed general experimental procedure for the ligand-free cyanation of aryl halides:

A solution of appropriate aryl halides **1** (1 mmol), $K_4[Fe(CN)_6].3H_2O$ (0.2 mmol) and K_2CO_3 (1.2 mmol) in DMF (3 mL), Ni-γAl_2O_3 (6 mol%) was added and stirred at 120°C for

View Article Online
DOI: 10.1039/D5MA00879D

the specified time. TLC was used to check the improvement of the reaction. The reaction mixture was cooled to room temperature once the reaction was finished. The product was then dissolved by adding 15 mL of ethyl acetate. The catalyst was removed by simple filtration. The recovered catalyst was thoroughly washed using ethyl acetate, followed by H_2O. Ethyl acetate was used several times to extract the aqueous part. The organic extracts were washed using water and dried on anhydrous Na_2SO_4. The product **2** was produced by evaporating the solvent at lowered pressure. Then it was further purified by column chromatography of silica gel with EtOAc-hexane as eluent.

2.3. Antioxidant Activity of Ni-γAl$_2$O$_3$:

Antioxidant activity of the synthesized Ni-γAl_2O_3 nanocatalysts was assessed using DPPH free radical scavenging assay.[25] 200 µL of a DPPH methanol solution was mixed with a different concentration of the samples (200, 100, 80, 40, 10 mg/ mL) followed by the incubation at 37°C for 30 min and absorbance was noted at the wavelength of 517 nm using (UV-VIS dual beam spectrophotometer). The reduction capacity was estimated in terms of ascorbic acid per mg. DPPH free radical scavenging potential (in percentage) was estimated by using the following equation.

$$\text{DPPH free radical Scavenging activity (\%)} = (A_{control}\text{-}A_{sample}) / A_{control} \times 100$$

2.4. Antibacterial Assay of Ni-γAl$_2$O$_3$:

2.4.1. Bacterial Strains:

Staphylococcus aureus ATCC25923 (Gram-positive) and *Escherichia coli* (Gram-negative) were used to study the antibacterial activity of Ni-γAl_2O_3. All these strains were cultured on nutrient agar plate.

2.4.2. Agar-Well Diffusion Method:

Antibacterial activity was assessed using agar well diffusion method. The bacterial strains were allowed to grow in Mueller-Hinton broth and 100µl of each bacterial suspension were spread over the Mueller-Hinton agar plate. 40µl of aforementioned Ni-γAl_2O_3 NPs (dissolved in 10% DMSO) was poured into the well present in the plate. DMSO was used as the negative control. All the plates were incubated at 37°C for overnight. After 24 hrs zone of inhibition was measured.[26] This assay was performed in triplicate and the observations are stated as mean ± SD.

View Article Online
DOI: 10.1039/D5MA00879D

2.5. Minimum Inhibitory (MIC) and Minimum Bactericidal Concentrations (MBC) Determination:

The minimum inhibitory was performed using dilution method. Ni-γAl_2O_3 NPs was diluted to attain the concentrations of 250, 240, 230, 220, 210, 205, 200, 195, 190 mg/mL respectively. 100 µL of respective bacterial suspension (10^5 CFU/mL) was spread over Mueller–Hinton agar plate followed by the addition of 40 µl of each dilution of Ni-γAl_2O_3 NPs to the respective wells in the plate. After that these plates were incubated at 37 °C for 24-48 hrs. Lowest concentration of Ni-γAl_2O_3 NPs that produce clearing zone was denoted as MIC value whereas the concentration that killed all bacterial cells was considered as MBC (minimum bactericidal concentration).

3. RESULTS AND DISCUSSION

3.1. Catalyst Characterization:

The FTIR spectra of γAl_2O_3 and synthesized Ni-γAl_2O_3 nanocatalyst were recorded in Figure 2. The FTIR spectra of γAl_2O_3 displayed the broad bands in the 3620-3032 cm^{-1} region, because of the existence of several hydroxyl groups on the γAl_2O_3 surfaces. Moreover, the FTIR spectra of γAl_2O_3 showed absorption peaks at 2090, 1966, 1639 cm^{-1} which are assigned to the bending mode of vibrations of adsorbed water molecules.[27] However, the intensities of these bands were reduced in the FTIR spectrum of the synthesized Ni-γAl_2O_3 nanocatalyst. These findings suggested the effective encapsulation of the metal into the pores of γAl_2O_3. The similar IR peaks at 1448 cm^{-1}, 1159 cm^{-1}, 1072 cm^{-1} in the γAl_2O_3 and 1460 cm^{-1}, 1162 cm^{-1}, 1078 cm^{-1} in the synthesized Ni-γAl_2O_3 nanocatalyst were also observed. This observation showed the effective formation of Ni-γAl_2O_3 nanocatalyst through the complexation as well as the stabilization of nanoparticles into the pore of γAl_2O_3. The FTIR spectra of Ni-γAl_2O_3 nanocatalyst exhibited the absorption peaks at 736 cm^{-1}, 619 cm^{-1}, and 495 cm^{-1} due to the stretching and bending vibrations between Ni-O, Ni-Al and Al-O bonds.[28]

View Article Online
DOI: 10.1039/D5MA00879D

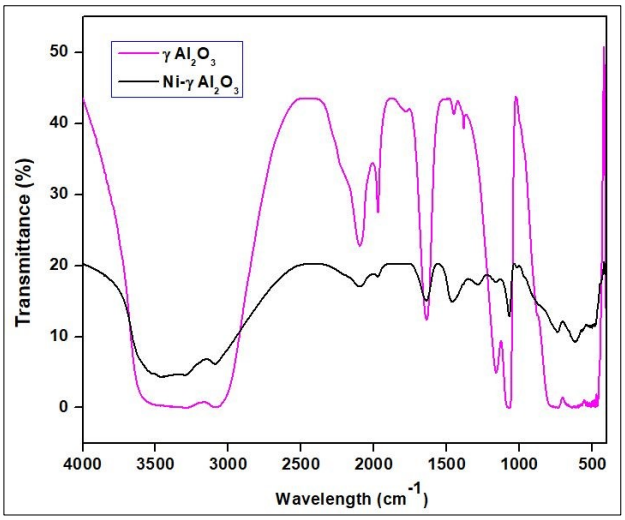

FIGURE 2 FTIR analysis of γAl_2O_3 and synthesized Ni-γAl_2O_3 nanocatalyst.

We performed the powdered X-ray diffraction analysis of the prepared Ni-γAl_2O_3 nanocatalyst to determine the crystallinity of our prepared catalyst. The X-ray diffraction patterns of the prepared Ni-γAl_2O_3 catalysts are displayed in Figure 3. The diffraction peaks exhibit that Al_2O_3 exists in gamma (γ) crystalline phase. The intensity of the peaks confirms that the particles are crystalline in nature. The appearance of diffraction peaks at $2\theta = 44.5^o$ and $2\theta = 51.7^o$ can be ascribed to the Ni (111) and Ni (200) crystalline planes respectively. These characteristic peaks also indicate the metallic nickel phase with fcc structure. This is also consistent with the reported literature.[29] The characteristic 2θ values of the nickel also revealed that the Ni^{2+} ions completely reduced to Ni^0 and the synthesized Ni^0 incorporated within the pores of γAl_2O_3 support.

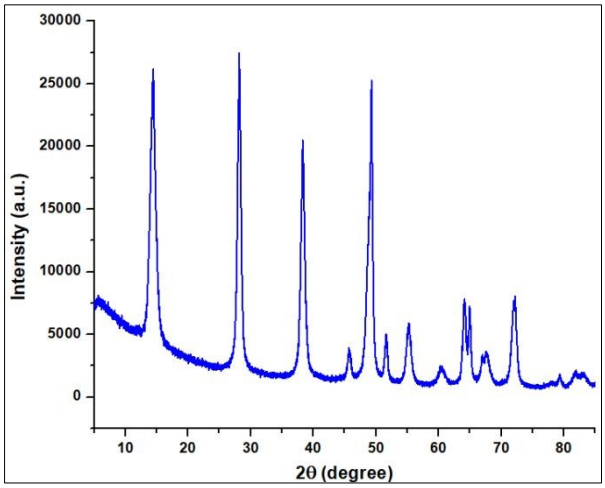

FIGURE 3 X-ray diffraction analysis of the synthesized Ni-γAl_2O_3 nanocatalyst.

View Article Online
DOI: 10.1039/D5MA00879D

The TEM and HRTEM images of the synthesized Ni-γAl_2O_3 nanocatalyst are illustrated in Figures 4. The TEM image of synthesized Ni-γAl_2O_3 nanocatalyst discloses the formation of a layered structure, suggesting a well-defined architecture (Figure 4a). Moreover, a good dispersion of metallic Ni on the surfaces of γAl_2O_3 support were observed in the structure of Ni-γAl_2O_3 nanocatalyst. Figures 4b and 4c indicate that the Ni nanoparticles exhibit an average size of 4-7 nm, demonstrating the nanoscale diameter of the active metal component. Remarkably, the HRTEM image in Figure 4c revealed the clear lattice fringes, further confirming the well dispersion and crystallinity of the synthesized nanomaterials on the surfaces of γAl_2O_3 support. Figure 4c also exhibits the lattice fringe distances of 0.20 and 0.17 nm, which can be attributed to the d-spacing values of the metallic Ni (111) and Ni (200) respectively.[30] Besides, the SAED (selected area electron diffraction) pattern substantiated the crystalline structure (Figure 4d), showing distinct diffraction spots, which further established the well-ordered arrangement and high crystallinity of the Ni-γAl_2O_3 nanocatalyst.

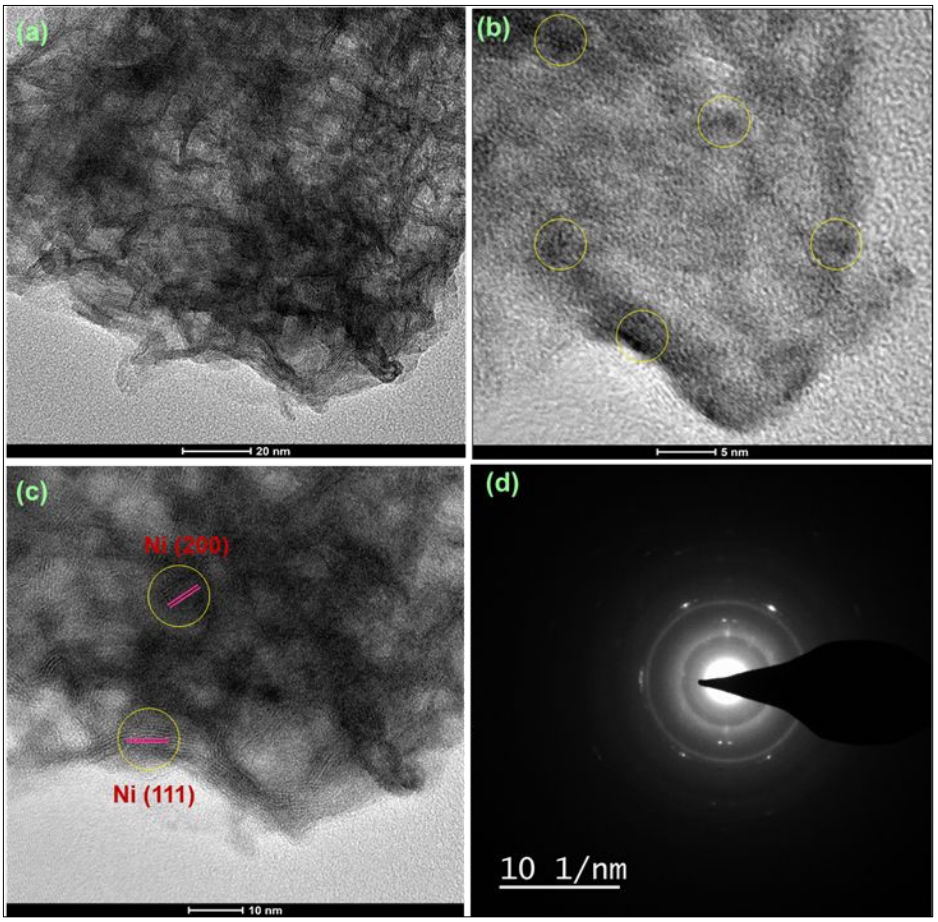

FIGURE 4 TEM and HRTEM images (a,b,c) and SAED pattern (d) of synthesized Ni-γAl_2O_3 nanocatalysts.

View Article Online
DOI: 10.1039/D5MA00879D

We next recorded the scanning electron microscopy (SEM) images of the prepared Ni-γAl_2O_3 catalyst which are depicted in Figure 5 (a-d). The results showed that the synthesized Ni-γAl_2O_3 catalyst displays a distinctly crystalline structure. Furthermore, the nanoparticles were irregularly distributed on the γAl_2O_3 support, which revealed a non-uniform arrangement. This irregularity could have an impact on the catalytic performance and efficiency of the nanocatalysts in a variety of catalytic applications. This finding is also corroborated by the aforesaid TEM images.

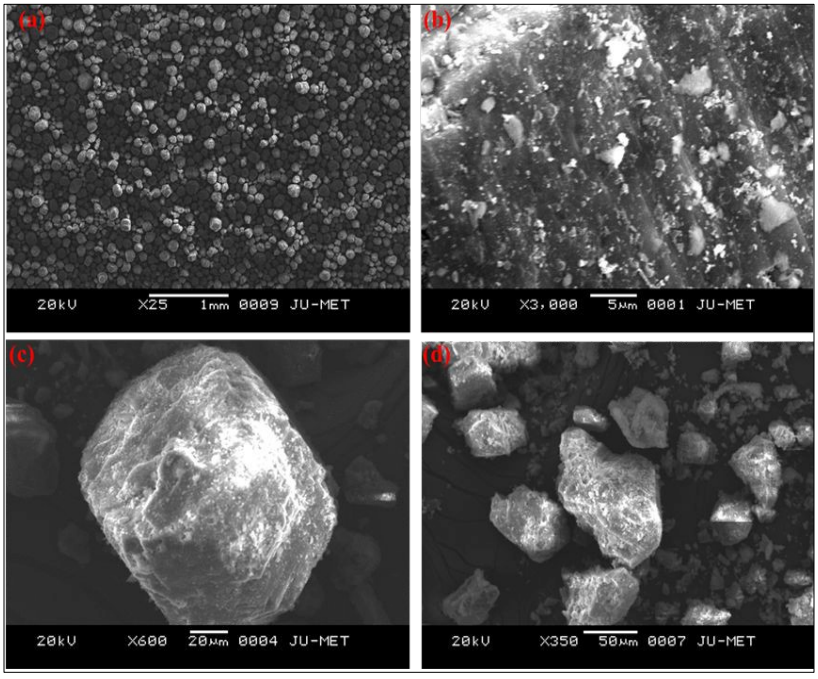

FIGURE 5 Scanning electron microscopy (SEM) images (a,b,c,d) of synthesized Ni-γAl_2O_3 nanocatalysts.

To investigate the elemental composition of the prepared Ni-γAl_2O_3 nanocatalyst, EDX (Energy dispersive X-ray spectroscopy) study was also investigated. Figure 6 showed the elemental peaks, which correspond to Ni, Al and O in the synthesized Ni-γAl_2O_3 catalyst. Besides, the elemental mapping images of the synthesized Ni-γAl_2O_3 catalyst were also carried out. The distribution of Ni, Al, and O elements was also observed by a mapping study, and well-arranged distributions of each element were also seen in the synthesized Ni-γAl_2O_3 nanocatalyst (Figure 7).

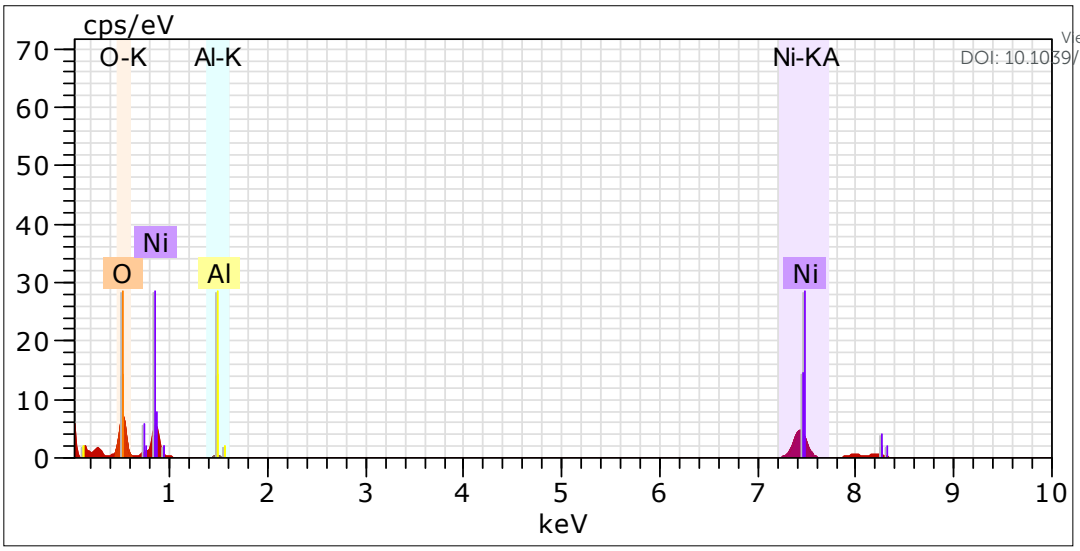

FIGURE 6 Energy dispersive X-ray spectroscopy analysis of Ni-γAl_2O_3 nanocatalyst

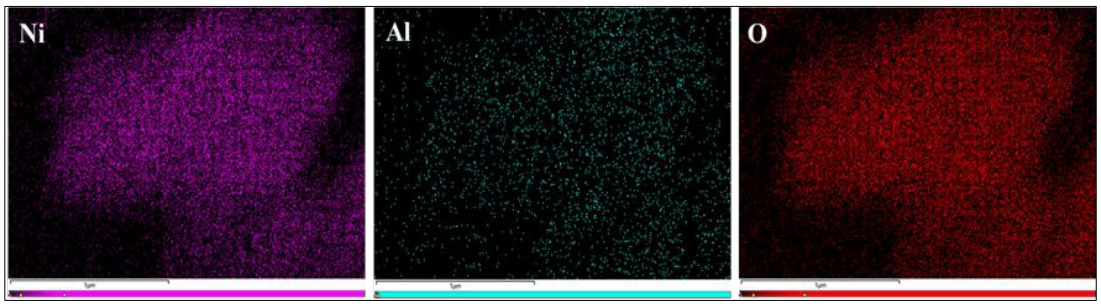

FIGURE 7 Elemental mapping images of synthesized Ni-γAl_2O_3 nanocatalyst

The N_2 adsorption-desorption study of the synthesized Ni-γAl_2O_3 catalyst (Figure 8a) demonstrates a type IV isotherm, supporting the presence of a mesoporous structure. BET analysis exhibited a high specific surface area of 173 m^2 g^{-1}, confirming the porous γAl_2O_3 support and homogeneous distribution of Ni species. The BJH desorption pore-size distribution (Figure 8b) reveals a predominant mesopore population centered at around 4 nm as well as a secondary broader distribution around 7-8 nm, confirming the bimodal mesoporosity of the Ni-γAl_2O_3 catalyst. Such a large high surface area and accessible mesopores are expected to facilitate the effective diffusion of aryl halides and cyanide released from $K_4[Fe(CN)_6]\cdot 3H_2O$ to the active Ni sites, thereby corroborating the observed catalytic efficiency in the cyanation of aryl halides.

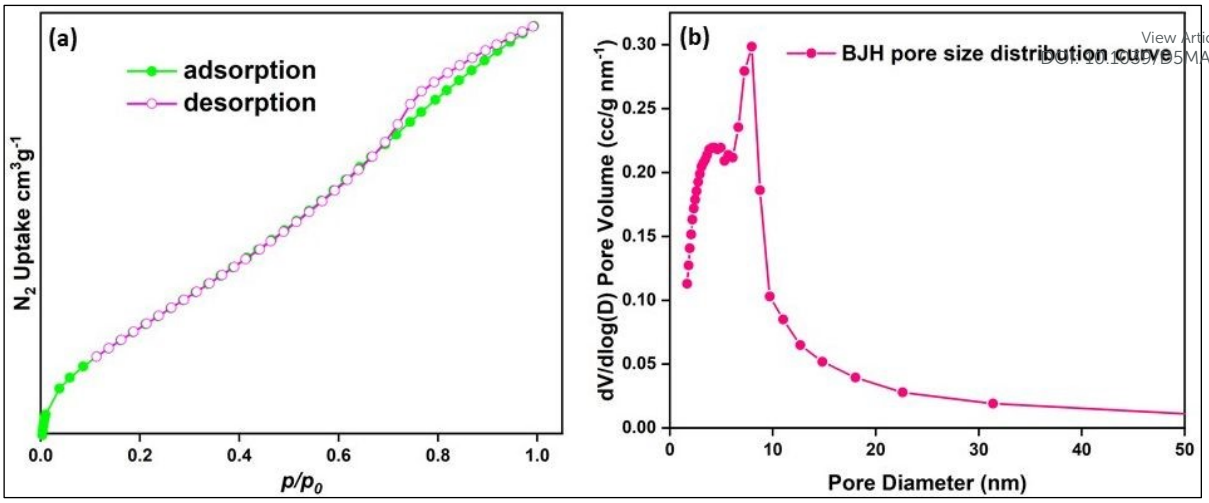

FIGURE 8 N_2 adsorption/desorption isotherm (a) and pore size distribution (b) of synthesized Ni-γAl_2O_3 nanocatalyst.

Thermogravimetric analysis (TGA) was conducted to examine the thermal behavior of the as-synthesized Ni-γAl_2O_3 catalyst. The TGA curve (Figure S1, Supporting Information) shows a gradual multi-step weight loss (approximately ~12 wt% total) between 25°C and 600°C. The first weight loss (4.26%) up to ~200°C is associated with the elimination of physically adsorbed moisture and residual water desorption from the high-surface-area of γAl_2O_3 support. The second weight decrease (4.17%) observed between ~200 °C and 385°C is assigned to the decomposition of residual organic species originating from acetylacetonate ligand, PEG-400 and hydrazine used during synthesis. The last weight loss (3.71%) between ~385°C and 520°C is attributed to the oxidation of metallic Ni(0) nanoparticles to NiO on the γAl_2O_3 surface. Above 520 °C, the TGA curve remains essentially stable, demonstrating the complete elimination of volatile species and indicating the high thermal stability of the γ-Al_2O_3 support. Overall, the TGA analysis validates the effective formation of Ni-γAl_2O_3 catalyst, successful elimination of most organic residues, and excellent thermal stability of the Ni-γAl_2O_3 catalyst.

These detailed characterizations emphasize the unique applicability of the synthesized Ni-γAl_2O_3 nanocatalyst for a variety of catalytic applications due to its unusual crystalline characteristics.

3.2. Catalytic Activity of the Ni-γAl_2O_3 Nanocatalyst:

The catalytic efficiency of Ni-γAl_2O_3 was investigated in the cyanation of aryl halides (such as aryl iodides, aryl bromides and aryl chlorides) using readily available, non-toxic, and

View Article Online
DOI: 10.1039/D5MA00879D

cost-effective $K_4[Fe(CN)_6].3H_2O$ as a green cyanide source. To achieve optimal conditions, several control experiments were investigated using 4-iodotoluene **1a** (1 mmol) as the model substrate and $K_4[Fe(CN)_6].3H_2O$ as the safe cyanide source in the presence of different bases in several solvents at various temperatures with the alteration of catalyst amount and reaction time (Table 1).

TABLE 1 Ni-γAl_2O_3 catalyzed optimization of reaction conditions[a]

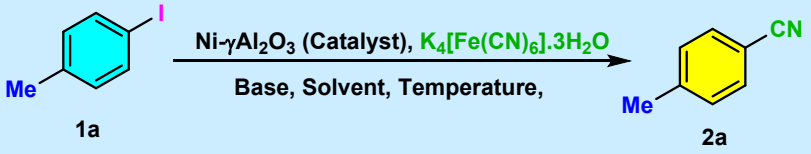

1a 2a

Entry	Catalyst (mol%)	Base (mmol)	Solvent (mL)	Temperature (°C)	Time (h)	Yield[b] (%)
1	--	--	DMF	Reflux	14h	--
2	--	K_2CO_3	DMF	Reflux	14h	--
3	2	--	DMF	Reflux	14h	Trace
4	4	K_2CO_3	DMF	120°C	12h	68
5	5	K_2CO_3	DMF	120°C	12h	74
6	**6**	**K_2CO_3**	**DMF**	120°C	**12h**	**92**
7	7	K_2CO_3	DMF	120°C	12h	93
8	6	Na_2CO_3	DMF	120°C	12h	85
9	6	NaOH	DMF	120°C	12h	22
10	6	KOH	DMF	120°C	12h	27
11	6	Et_3N	DMF	120°C	12h	Trace
12	6	Pyridine	DMF	120°C	12h	Trace
13	6	K_2CO_3	DMSO	Reflux	12h	68
14	6	K_2CO_3	Toluene	Reflux	12h	--
15	6	K_2CO_3	Xylene	Reflux	12h	--
16	6	K_2CO_3	H_2O	Reflux	12h	--
17	6	K_2CO_3	CH_3CN	Reflux	12h	29
18	6	K_2CO_3	EtOAc	Reflux	12h	35

[a]Reaction conditions: **1a** (1.0 mmol), $K_4[Fe(CN)_6].3H_2O$ (0.2 mmol); base (1.2 mmol), solvent (3 mL), catalyst and temperature (as indicated) under ambient condition. [b]Isolated yield.

The reaction initially failed without using Ni-γAl_2O_3 and base (Entry 1) and in the presence of a base (Entry 2), no nitrile product **2a** was isolated in all the cases. However, in the absence of base, only a small amount of **2a** was observed after 14 h when the reaction

View Article Online
DOI: 10.1039/D5MA00879D

was examined using 2 mol% of catalyst under reflux condition in DMF solvent (Entry 3). Using 4 mol% of Ni-γAl_2O_3 catalyst and 1.2 mmol of K_2CO_3 base (Entry 4), the conversion reached 68% within 12 h at 120°C. After increasing the catalyst concentration (5 mol%), the conversion was improved to 74% after 12 h (Entry 5). Satisfactory outcome was found after 12h using Ni-γAl_2O_3 (6 mol%) and K_2CO_3 (1.2 mmol) (Entry 6). Excess catalyst exceeding 6 mol% showed no further increase in conversion rate (Entries 6-7). When K_2CO_3 was replaced with Na_2CO_3, the reaction yield was slightly reduced to 85% (Entry 8). Strong bases such as NaOH (Entry 9) and KOH (Entry 10) reduced the yield drastically. Treatment of organic bases such as Et_3N (Entry 11) and pyridine (Entry 12) resulted in only trace amounts of product under the similar reaction conditions. Finally, the K_2CO_3 was turned out to be the most effective base in DMF medium at 120°C for the cyanation reaction. Moreover, different types of solvents were also screened. The efficiency of the reaction slightly decreases when DMSO is used in place of DMF (Entry 13). Other solvents such as toluene, xylene, and water showed negative results (Entries 14-16). Inferior performance was obtained when CH_3CN and EtOAc were used as the reaction medium in the cyanation of aryl halides (Entries 17-18). Therefore, the conditions, as delineated in Entry 6, were selected as the optimized reaction condition to investigate the substrate scope and ensure the practical applicability of this reaction. The aforesaid protocol did neither occur with γAl_2O_3 alone nor with Ni nano without γAl_2O_3 nor with Ni(acac)$_2$-γAl_2O_3. The importance of Ni-γAl_2O_3 for this cyanation reaction is highly crucial due to its high stability and better catalytic activity.

To establish the general applicability of this protocol, the optimized reaction conditions have been employed for the cyanation of aryl iodides / bromides / chlorides bearing several electron-withdrawing and electron-donating substituents at various places of the benzene. The corresponding nitriles were produced with good to high yields. The results are presented in Table 2.

TABLE 2 Ni-γAl_2O_3 catalyzed cyanation of aryl halides using $K_4[Fe(CN)_6].3H_2O$ as the green cyanating agent[a]

Entry	Substrate	Product	Time (hrs)	Yield[b] (%)
		Cyanation of aryl iodides		
1	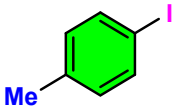 **1a**	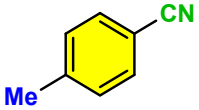 **2a**	12	92

View Article Online
DOI: 10.1039/D5MA00879D

2	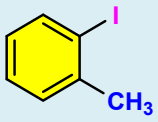 **1b**	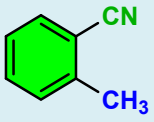 **2b**	12	88
3	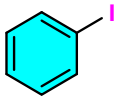 **1c**	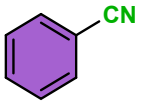 **2c**	12	91
4	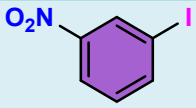 **1d**	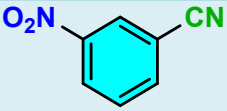 **2d**	10	94
5	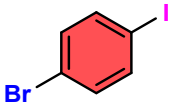 **1e**	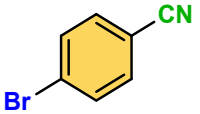 **2e**	12	93
6	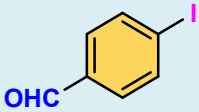 **1f**	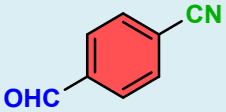 **2f**	12	92
Cyanation of aryl bromides				
7	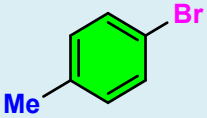 **1g**	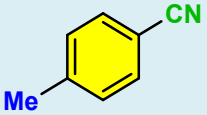 **2a**	12[c] / 18[d]	88[c] / 32[d]
8	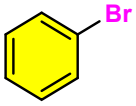 **1h**	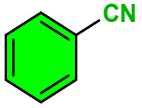 **2c**	12[c] / 18[d]	90[c] / 35[d]
9	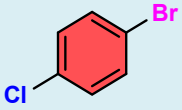 **1i**	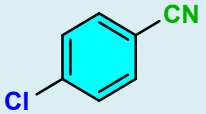 **2g**	12[c] / 18[d]	88[c] / 30[d]
10	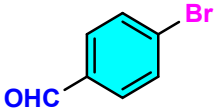 **1j**	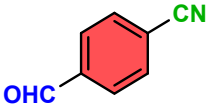 **2f**	12[c] / 18[d]	92[c] / 33[d]
11	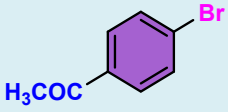 **1k**	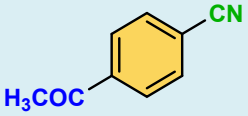 **2h**	12[c] / 18[d]	91[c] / 30[d]
12	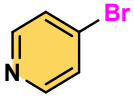 **1l**	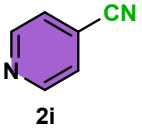 **2i**	12[c] / 18[d]	80[c] / 25[d]

Cyanation of aryl chlorides				
13	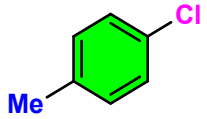 **1m**	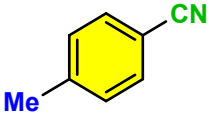 **2a**	12[c] / 22[d]	76[c] / 22[d]
14	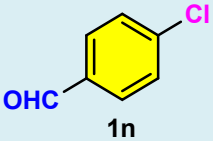 **1n**	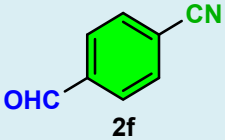 **2f**	12[c] / 22[d]	73[c] / 19[d]
15	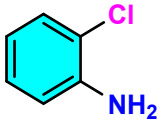 **1o**	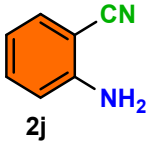 **2j**	12[c] / 22[d]	78[c] / 23[d]
16	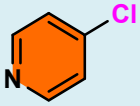 **1p**	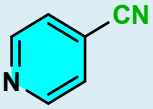 **2i**	12[c] / 22[d]	76[c] / 22[d]

[a]Reaction conditions: **1a** (1 mmol), $K_4[Fe(CN)_6].3H_2O$ (0.2 mmol), K_2CO_3 (0.5 mmol), Ni-γAl_2O_3 (6 mol%), DMF (3 mL) at 120°C. [b]Yield states to the isolated pure product. [c]In presence of additive (KI) (1.0 mmol) for bromo and chloro compounds. [d]In absence of additive (KI) (1.0 mmol) for bromo and chloro compounds.

As evident from Table 2, a wide variety of aryl iodides (**1a-1f**) bearing electron-donating and electron-withdrawing substituents were transformed into the products (**2a-2f**) in good to excellent yield. Cyanation of *ortho*-substituted compounds such as 2-iodotoluene (**1b**) afforded the corresponding nitrile (**2b**) under the optimized reaction conditions with slightly lower yield due to steric reasons. 3-nitroiodobenzene (**1d**) smoothly cyanated into their corresponding nitrile (**2d**) with 94% yield within a shorter reaction time without interfering $–NO_2$ groups. The aforesaid protocol displayed selectivity for the cyanation of 4-bromoiodobenzene (**1e**) which selectively produces 4-bromobenzonitrile (**1e**) with excellent yield without hampering the C-Br bond. This could be due to the low bond dissociation energy of the C-I bond compared to C-Br bond. This reaction is also highly effective for the substrate bearing a highly reducible group. 4-iodobenzaldehyde (**1f**) also responded efficiently to provide the corresponding nitrile **2f** with good yield within 12h. The formation of **2f** was confirmed by the ^1H and ^{13}C NMR spectroscopy. The ^1H NMR spectrum of **2f** showed the existence of -CHO group which appeared as a singlet at δ 10.07 and two doublets at δ 7.975 because of the aromatic ortho protons with respect to –CHO group and at δ 7.825 because of the aromatic ortho protons with respect to the –CN group. The ^{13}C NMR spectrum

View Article Online
DOI: 10.1039/D5MA00879D

of **2f** displayed the appearance of two main signals at δ 190.7 and δ 117.8, demonstrating the existence of both –CHO and –CN groups respectively. We next extended the optimized reaction conditions for a wide variety of aryl bromides and aryl chlorides. The corresponding nitrile was observed with lower yield even after a longer reaction time. The bond dissociation energy of C-X (X = Cl, Br, I) is C-Cl > C-Br > C-I. Therefore, the oxidative addition of Ni on aryl bromides as well as aryl chlorides is complicated when compared with aryl iodide. Hence, the cyanation of aryl bromides (**1g-1l**) and aryl chlorides (**1m-1p**) showed lower yield. However, the reaction yield was achieved comparatively high when the reaction was carried out using iodide ion. The main role of iodide ion is to catalyze the construction of aryl iodide from aryl bromides and aryl chlorides, and therefore the in situ cyanation reaction takes place, as reported by Buchwald et al.[31] We observed that 1.0 mmol of KI is necessary to endorse the incorporation of iodide into aryl bromides as well as aryl chlorides. Therefore, both differently substituted aryl bromides and aryl chlorides readily furnished their cyanated products with moderate to good yield in the presence of 1.0 mmol of KI as an additive. This is an immensely essential feature of the present method in comparison to reported methods, where no such additional reactivity of aryl bromides and aryl chlorides was observed.[17a,17b,17c,17d]

The plausible reaction pathway for this Ni-γAl_2O_3 catalysed cyanation of aryl halides is presented in Scheme 2.[32a,32b,32c] The oxidative addition of aryl halides to the nickel metal seems to be the initiation step of this catalytic reaction, and therefore metallic nickel oxidised to Ni (II) species (A). Then the exchange of ligand from the inside coordination sphere of $K_4[Fe(CN)_6]$ to the Ni(II) species (B) of the catalyst takes place through the transmetallation process. Finally, the reductive removal stage resulted in the formation of arylnitriles with the regeneration of the metallic nickel catalyst.

View Article Online
DOI: 10.1039/D5MA00879D

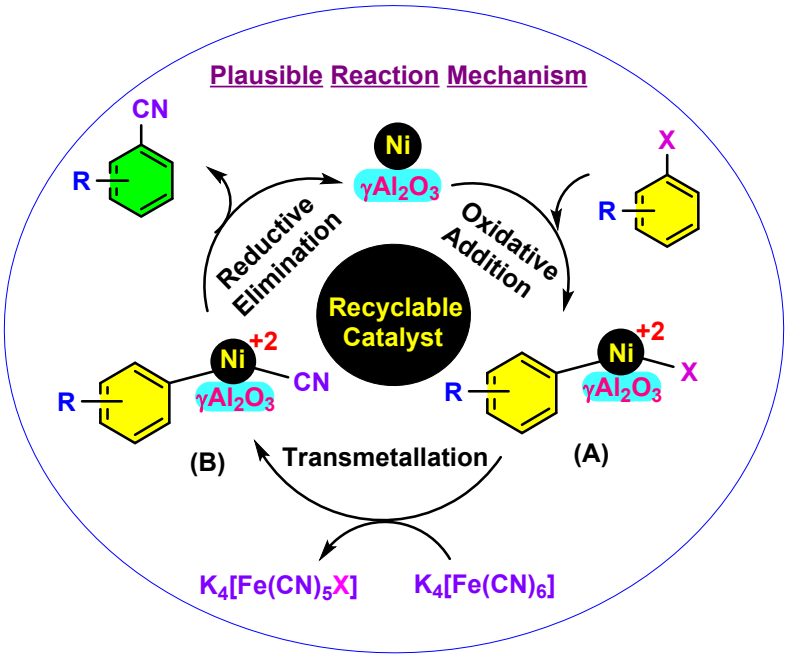

SCHEME 2 Plausible mechanism for the Ni-γAl_2O_3 catalyzed cyanation of aryl halides.

To design a sustainable protocol, the recoverability and reusability[33a,33b,33c,33d] of the catalyst is highly essential in terms of a green perspective. Therefore, the recycling test of our prepared Ni-γAl_2O_3 catalyst was performed using 4-iodotoluene **1a** (1 mmol), $K_4[Fe(CN)_6].3H_2O$ (0.2 mmol), K_2CO_3 (1.2 mmol), Ni-γAl_2O_3 (6 mol%), DMF (3 mL) at 120°C. We separated the Ni-γAl_2O_3 catalyst by simple filtration after the end of the reaction. The extraction of crude product from the filtrate was carried out using EtOAc solvent. The recovered catalyst was thoroughly washed using ethyl acetate, followed by H_2O. Then the recovered Ni-γAl_2O_3 catalyst was dried at 120°C for one hour. The recovered Ni-γAl_2O_3 catalyst was then applied for a series of catalytic reactions with not much variation in yield (Figure 9a). The significant recyclability of this Ni-γAl_2O_3 catalyst encouraged us to further analyse the characterization study of the recycled Ni-γAl_2O_3 to confirm their stability. Therefore, SEM and TEM analyses of the recycled Ni-γAl_2O_3 were investigated (Figures 9b and 9c). The aforesaid studies demonstrate that the structural features of the Ni-γAl_2O_3 catalyst were relatively stable during this investigation. Moreover, ICP-OES analysis was carried out to determine the actual Ni loading and investigate the stability of the Ni-γAl_2O_3 catalyst. The fresh catalyst contained 5.1 wt% Ni, whereas the recycled catalyst (after the 5th catalytic run) retained 5.04 wt% Ni, showing only 0.06% metal leaching. This negligible loss indicates that Ni remains well-dispersed and firmly anchored on the γ-Al_2O_3 support.

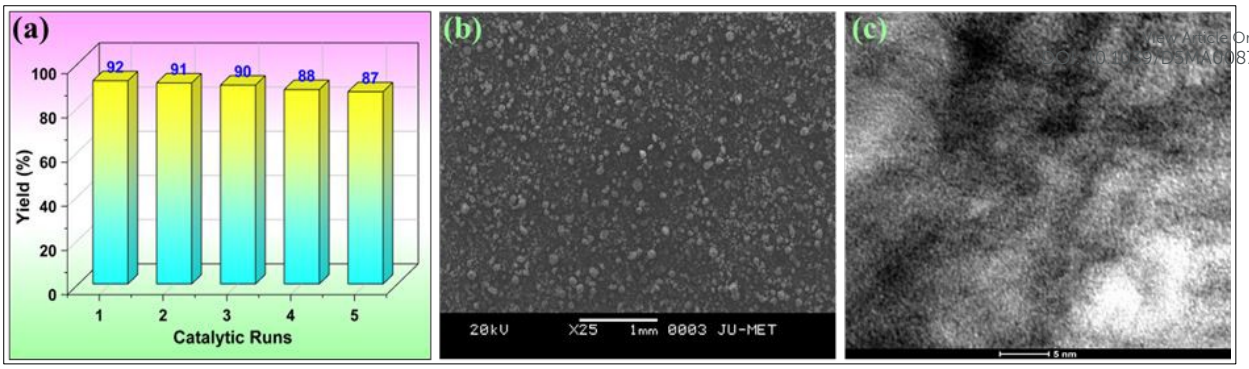

FIGURE 9 (a) Recycling test of Ni-γAl_2O_3 catalyst, (b) SEM image of Ni-γAl_2O_3 (after recycled 5 times), and (c) TEM image of Ni-γAl_2O_3 (after recycled 5 times).

3.3. Hot Filtration Experiment (Sheldon's Test) of the Ni-γAl_2O_3 Nanocatalyst:

Furthermore, the hot filtration test[34a,34b] (Sheldon's test) was carried out to establish the heterogeneous nature of Ni-γAl_2O_3 catalyst with 4-iodotoluene (**1a)** as the model substrate. When 32% conversion of the **1a** was observed after 3h, the separation of Ni-γAl_2O_3 catalyst was carried out through filtration under hot conditions. Then the reaction without a catalyst was continued for 14 h. No more transformation of **1a** occurred (Figure 10). This experiment revealed that there were no catalytically active species in the remaining reaction mixture. Therefore, the heterogeneous nature of Ni-γAl_2O_3 was successfully proven.

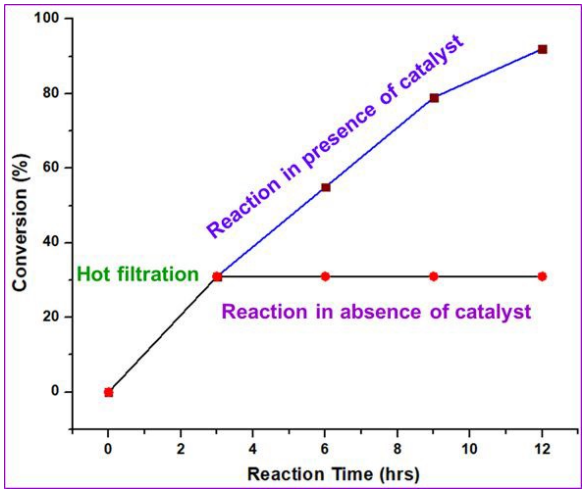

FIGURE 10 Hot-filtration test of Ni-γAl_2O_3 catalyst using **1a** (1 mmol), $K_4[Fe(CN)_6].3H_2O$ (0.2 mmol), K_2CO_3 (1.2 mmol), Ni-γAl_2O_3 (6 mol%), DMF (3 mL) at 120°C under ambient condition.

DOI: 10.1039/D5MA00879D

3.4. Comparative Efficiency of Ni-γAl_2O_3 Catalyst with Other Reported Ni-based Catalysts:

Table 3 summarizes the comparative overview of previously reported Ni-catalyzed cyanation reactions (Entries 1-5) and compares the efficiency of our synthesized Ni-γAl_2O_3 nanocatalyst (Entry 6). The earlier reported methods (Entries 1- 4) employ homogeneous nickel catalytic procedures in combination with harmful cyanating agents such as ^{t}BuCN,[35a] BrCN,[35b] or the relatively less hazardous 1,4-dicyanobenzene.[35c] Despite the potential efficiency of these homogeneous systems, the necessity of expensive reagents and strong additives,[35c,35d] requirements of an inert atmosphere and photochemical activation,[35c] laborious preparation[35d] and poor recyclability of the catalysts[35a,35b,35c,35d] were the serious limitations of these methods. Although $NiFe_2O_4$ catalyst demonstrated the good catalytic activity and recyclability of the catalyst (Entry 5), its scope is limited due to the employment of highly toxic NaCN as the cyanating agent.[35e] In this context, our developed Ni-γAl_2O_3 nanocatalyst represents an economically efficient and operationally simple catalytic system for the cyanation reactions with the utilization of $K_4[Fe(CN)_6].3H_2O$ as a safe and eco-friendly cyanide source. The excellent catalytic efficiency of Ni-γAl_2O_3 nanocatalyst ensures the good dispersion of nickel species on the γAl_2O_3 support suggesting the strong metal-support interaction. Importantly, the Ni-γAl_2O_3 catalyst can be efficiently recycled and reused for five successive runs without substantial loss of efficiency, signifying its higher stability in comparison to previously reported Ni-based catalytic systems. Moreover, the attractive features, such as the new catalyst design, green cyanation reaction**,** high efficiency, and excellent recyclability, which clearly distinguish the present catalytic methodology from earlier Ni-based catalytic systems.

Table 3 Comparative Efficiency of Ni-γAl_2O_3 Catalyst with Other Ni-Based Catalysts for the Cyanation of Aryl Halides[a]

Entry	Catalyst	Cyanating Agent	Reaction Conditions	Yield (%)	Catalyst Type & Recyclability	Ref
1	$NiBr_2$ / PCy_3 / Mn	^{t}BuCN	$NaHCO_3$, Toluene, 150°C, 22h	56%	Homogeneous, Not reported	35a
2	$NiCl_2$.1,10-phen/Zn	BrCN	Dioxane, 50°C, 12h	84%[b]	Homogeneous, Not reported	35b
3	NiI_2, dtbbpy, Purple light (390-395 nm)	1,4-dicyano benzene	DBU, TMSBr, (TMS)SiH_3, Toluene, Ar atm., 50°C, 24h	79%[c]	Homogeneous, Not reported	35c

4	$Ni(PPh_3)_2$(1-Naph)Cl, JosiPhos	$K_4[Fe(CN)_6].3H_2O$	TBAHS, DIPEA, nBuOAc:H_2O, 95°C,	83%[d]	Homogeneous, Not reported	35d
5	$NiFe_2O_4$	NaCN	K_2CO_3, DMF, 100 °C, 17 min.	92%	Heterogeneous, 5 cycles	35e
6	Ni-γAl_2O_3	$K_4[Fe(CN)_6].3H_2O$	K_2CO_3, DMF, 120 °C, 12h	91%	Heterogeneous, 5 cycles	This work

[a]Iodobenzene was used as the model substrate, [b]Yield of 4-methoxyiodobenzene, [c]Yield of 4-methoxybromobenzene, [d]Yield of 3-bromo benzaldehyde.

3.5. *Antioxidant Activity of Ni-γAl_2O_3 Nanocatalysts:*

In the present study Ni-γAl_2O_3 nanoparticles had shown moderate antioxidant activity and maximum antioxidant activity (68.17%) was attained at 200 mg/ml concentration (Figure 11). Previous literature also has shown their antioxidant activity.[36a,b] Antioxidant property exhibited by Ni-γAl_2O_3 nanoparticles might be due to their free radicals scavenging capacity to reduce oxidative stress. This might be attained by donation of electrons or hydrogen atoms for the neutralization of free radicals as well as redox active sites located on nickel nanoparticles. Beside this alumina also exhibits high surface area which plays an important role in free radicals scavenging capacity (antioxidant activity) through the promotion of the adsorption as well as interaction with free radicals.[36a,b] IC_{50} of ascorbic acid was 22.73 µg/mL while it was 146.69 mg/mL for Ni-γAl_2O_3 nanoparticles. This observation suggests that DPPH reduction capacity is less than that of ascorbic acid which was also reported earlier.[36b]

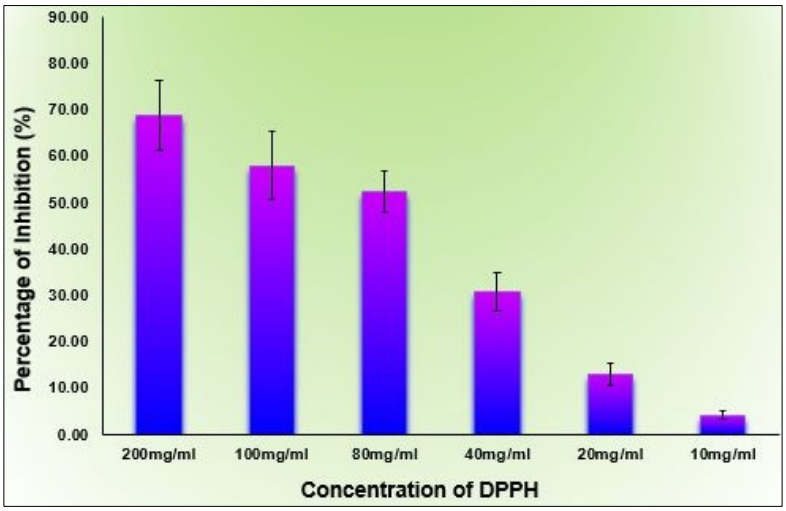

FIGURE 11 DPPH radical scavenging activity of Ni-γAl_2O_3 nanoparticles at different concentration

View Article Online
DOI: 10.1039/D5MA00879D

3.6. Antibacterial Activities of Ni-γAl_2O_3 Nanocatalysts:

The antibacterial activities of the Ni-γAl_2O_3 nanoparticles was tested against *Staphylococcus aureus* ATCC25923 (Gram-positive) and *Escherichia coli* (Gram-negative). The aforementioned Ni-γAl_2O_3 nanoparticles were found to be effective against both *Staphylococcus aureus* ATCC25923 and *Escherichia coli* (Figure 12). The zone of inhibition against *Escherichia coli* was 12±0.31 while it was 10±0.25mm in case *Staphylococcus aureus* ATCC25923 (Table 4). Inhibitory effect of Ni nanoparticles against both Gram-negative and Gram positive was also reported earlier by Angel Ezhilarasi et al.,[37a] Prabhu et al.,[37b] Rajith Kumar et al.[37c] Larger surface area, high reactivity of Ni NPs might boost and promote its antibacterial property (Bauer 1966). MIC values against *Escherichia coli* and *Staphylococcus aureus* ATCC25923 were 200 mg/mL and 205 mg/mL respectively while MBC values were 220 and 230 mg/mL respectively (Table 4). Lower MIC and MBC values of Ni nanoparticles against *Escherichia coli* in comparison to that of MIC and MBC values against *Staphylococcus aureus* ATCC25923 was also reported earlier.[38] Besides, previous literature also reported that inhibition of the growth of *E. coli* by Ni-Al_2O_3 nanoparticles was found to require 0.01 g/mL of Ni-Al_2O_3 nanoparticles.[38d]

Table 4 Zone of inhibition, MIC and MBC values of Ni-γAl_2O_3 nanoparticles

Nanoparticles	Bacterial strains	Zone of Inhibition (mm)	MIC values (mg/mL)	MBC values (mg/mL)
Ni-γAl_2O_3	*Escherichia coli*	12 ± 0.31	200	220
	Staphylococcus aureus ATCC25923	10 ± 0.25	205	230

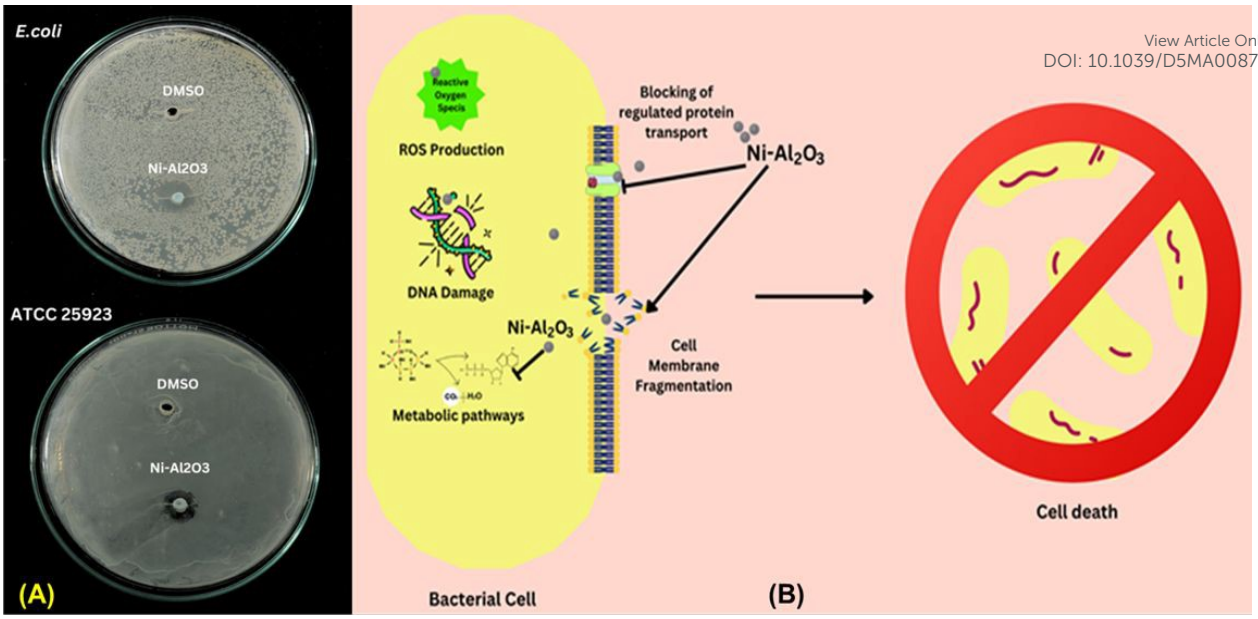

FIGURE 12 (A) Antibacterial activity of Ni-γAl_2O_3 nanoparticles against *Escherichia coli* and *Staphylococcus aureus* ATCC25923 which were grown on Mueller–Hinton agar plate at 37°C. DMSO was used as a negative control. (B) The plausible mechanism of action of Ni-γAl_2O_3 nanoparticles exhibiting antibacterial activity.

Additionally, a comparative table (Table S1, Supporting Information) has been presented to compare the antibacterial performance of our synthesized Ni-γAl_2O_3 nanocatalysts with the previously reported other metal-based nanocatalysts. However, the Ni-γAl_2O_3 nanocatalysts exhibited higher MIC and MBC values compared to conventional antibiotics. The absence of specific bioactive groups in the Ni-γAl_2O_3 nanocatalysts resulted in high MIC/MBC values, which exhibited poor membrane permeability along with less interaction with bacterial cell surfaces. The present study demonstrates that the pristine Ni-γAl_2O_3 catalyst displays baseline antibacterial efficacy. However, future progress could be accomplished through surface modification with bioactive phytochemicals, the introduction of synergistic metallic dopants, and the merging of the nanocatalyst with traditional antibiotics to improve membrane penetration and offer synergistic bactericidal properties.[1a,1b] These approaches will serve to substantially lower MIC/MBC values and extend catalyst utility in subsequent biological applications.

Antibacterial activity may be attributed by nickel nanoparticles inducing gaps and pits which make bacterial cell membrane to be fragmented. This fragmentation of bacterial membrane had been also reported by other researchers.[38a,38b,38c] Furthermore, the metals such

View Article Online
DOI: 10.1039/D5MA00879D

as Ni is effectively affected transport system of the bacteria by interacting with proteins to block regulated transport through the plasma and thus cause their death.[39] Beside this hyperactive property of Ni NPs due to unpaired electrons on the surface of Ni NPs underscores complex interactions with bacterial cellular components. Thus, Ni NPs causes the disruption of the metabolic pathways which leads to the death of the bacteria.[40] Moreover, Ni NPs has been found to generate oxidative stress in bacteria which is a pivotal mechanism for their antimicrobial property by damaging DNA, oxidation of protein and finally disrupting cell membrane as well.[41a,41b] For instance, destruction of bacterial cells confers the release of cellular content and cell death.[41b] Inhibitory effect of Ni-γAl_2O_3 nanoparticles against Gram-negative bacteria *Escherichia coli* was higher than the Gram-positive *Staphylococcus aureus* ATCC25923, which might be due to differences in the cell wall structure of Gram-negative and Gram-positive bacteria. Similar findings also showed by Angel Ezhilarasi et al.,[37a] Prabhu et al.,[37b] Rajith Kumar et al.[37c] Gram-negative bacteria had an outer layer of lipopolysaccharides and thin peptidoglycans that made easy nanoparticles to enter inside the cell. But, Gram-positive bacteria had a thick peptidoglycan layer covalently bonded teichoic and teichuronic acids acting as a protective layer.[42] A schematic diagram regarding the mechanism of action is given in Figure 12B.

4. CONCLUSION

The cyanation of aryl halides to aryl nitriles has been developed using economically supportable and operationally simple Ni-γAl_2O_3 as a heterogeneous catalyst and commercially available $K_4[Fe(CN)_6]$ as an eco-friendly cyanating agent. The reactions are not dependent on an inert atmosphere or a ligand. Several aryl iodides, bromides and chlorides bearing various functional moieties were well survived and associated with good to high yield in the aforesaid method. The synthesized Ni-γAl_2O_3 nanocatalysts could be recovered and recycled again without significantly reducing their efficacy. Moreover, the "hot filtration method (Sheldon's test)" was carried out to establish the heterogeneity of the catalyst. The present method attracts attention because of its procedural simplicity, significant catalytic durability and productivity, simple recovery, high recyclability, and survival of diverse functional groups in the reaction. In the present study Ni-γAl_2O_3 nanocatalysts were found to have moderate antioxidant activity, with maximum antioxidant activity (68.17%) attained at 200 mg/ml concentration. Ni-γAl_2O_3 nanocatalysts of the present study were found to inhibit

View Article Online
DOI: 10.1039/D5MA00879D

the growth of *Staphylococcus aureus* ATCC25923 (Gram-positive) and *Escherichia coli* (Gram-negative). But the zone of inhibition (12±0.31mm) against *Escherichia coli* was found to be higher than the zone of inhibition (10±0.25mm) against *Staphylococcus aureus* ATCC25923. Larger surface area, unique physiochemical property, high reactivity of Ni-γAl_2O_3 nanocatalysts might be responsible for their inhibitory effect against both Gram-negative and Gram-positive.

ACKNOWLEDGEMENT

A. K. Das gratefully acknowledges the Department of Science & Technology and Biotechnology, Govt. of West Bengal for financial grant (Grant No. 2147(Sanc.)/STBT-11012(25)/1/2024-ST SEC). S. Biswas gratefully acknowledges DST-SERB for financial grant (File No: SUR/2022/001437 dated 04.10.2023). Special thanks to Dr. M. Maji and Dr. S. Mondal for necessary assistance.

AUTHOR CONTRIBUTIONS

Asit Kumar Das: Conceptualization, Project administration, Writing-original draft preparation, Supervision. Md Sattar Ali: Methodology, Investigation, Data curation, Formal analysis. Arindam Misra: Methodology, Investigation, Data curation, Formal analysis. Md Sultan Saikh: Methodology, Investigation, Data curation, Formal analysis. Subhendu Dhibar: Resources, Data curation. Sumit Kumar Panja: Resources, Data curation. Aniruddha Das: Data curation, Validation, Formal analysis. Gourav Ghatak: Investigation, Biological Study. Lokesh Kumar Rathore: Resources, Data curation. Ashok Bera: Resources, Data curation. Sanjay Bhar: Editing, Writing and Review. Smritikana Biswas: Investigation, Biological Study, Writing-original draft preparation, Supervision.

CONFLICT OF INTEREST

This is to declare that there is no conflict of interest in this article.

DATA AVAILABILITY STATEMENT

The data that supports the findings of this study are available in the supplementary material of this article.

Notes and References:

1. (a) M. Binandeh, *Eur. J. Med. Chem. Rep.*, 2022, **6**, 100072; (b) M. Binandeh, *Bioinspired, Biomimetic and Nanobiomaterials*, 2023, **11**, 121-127; (c) A. Raghunath, and E. Perumal, *Int. J. Antimicrob. Agents* 2017, **49**, 137-152.
2. M. Rai, A. Yadav, and A. Gade, *Biotechnol. Adv.* 2009, **27**, 76-83.
3. J. J. Lin, W. C. Lin, S. D. Li, C. Y. Lin, and S. H. Hsu, *ACS Appl. Mater. Interfaces.* 2013, **5**, 433-443.
4. B. Le Ouay, and F. Stellacci, *Nano Today* 2015, **10**, 339-354.
5. P. Huo, *J. Ind. Eng. Chem.* 2018, **57**, 125-133.
6. R. Dadi, R. Azouani, M. Traore, C. Mielcarek, and A. Kanaev, *Mater. Sci. Eng. C* 2019, **104**, 109968.
7. R. A. Ulwali, H. Kh. Abbas, N. Yasoob, and H. A. Alwally, *Neuro Quantology* 2021, **19**, 42-52.
8. S. Debnath, S. Ghosh, S. Das, P. Das, S. Sarkar, and S. M. Mandal, *Journal of Basic Microbiology* 2016, **56**, 614-625.
9. (a) R. C. Larock, In Comprehensive Organic Transformations: a Guide to Functional Group Preparations; *Wiley-VCH: Weinheim, Germany*, 1989, 819; (b) A. Kleemann, J. Engel, B. Kutscher, and D. Reichert, Pharmaceutical Substances: Syntheses, Patents, Applications, 4th ed.; *Georg Thieme: Stuttgart*, 2001.
10. R. C. Larock, *Comprehensive Organic Transformations, 2nd ed*; Wiley: New York, 1999;
11. P. Anbarasan, T. Schareina, and M. Beller, *Chem. Soc. Rev.* 2011, **40**, 5049-5067.
12. (a) M. N. Janakirman, K. D. Watenpaugh, and K. T. Chong, *Bioorg Med Chem Lett.* 1998, **8**, 1237; (b) S. I. Murahashi, *Sci. Synth.* 2004, **19**, 345. Georg Thieme; (c) L. H. Jones, N. W. Summerhill, N. A. Swain, and J. E. Mills, *Med Chem Commun.* 2010, **1**, 309; (d) A. M. Sweeney, P. Grosche, D. Ellis, K. Combrink, P. Erbel, N. Hughes, F. Sirockin, S. Melkko, A. Bernardi, P. Ramage, N. Jarousse, and E. Altmann, *ACS Med. Chem. Lett.* 2014, **5**, 937.
13. (a) T. Sandmeyer, *Ber. Dtsch. Chem. Ges.* 1884, **17**, 1633; (b) T. Sandmeyer, *Chem. Ber.* 1884, **17**, 2650; (c) T. Sandmeyer, *Chem. Ber.* 1885, **18**, 1492; (d) T. Sandmeyer, *Chem. Ber.* 1885, **18**, 1946; (e) K.W. Rosenmund, and E. Struck, *Chem. Ber.* 1919, **2**, 1749.
14. (a) A. K. Das, and K. Sarkar, *New J. Chem.* 2025, **49**, 12898-12930; (b) A. Pramanik, A. K. Das, S. Bhar, and A. Ghatak, *ChemistrySelect*, 2025, **10**, e202500035; (c) S. Nandy, A. K. Das and S. Bhar, *Syn Commun.* 2020, **50**, 3326-3336; (d) A. Ghatak, A. K. Das, S. Bhar, and A. Pramanik, *J. Het. Chem.* 2025, **62**, 760-780.

15. (a) M. Sundermeier, A. Zapf, and M. Beller, *Eur. J. Inorg. Chem.* 2003, 3513-3526; (b) G. P. Ellis, and T. M. Romney-Alexander, *Chem. Rev.* 1987, *87*, 779; (c) V. V. Grushin, and H. Alper, *Chem. Rev.* 1994, **94**, 1047.

16. T. Kentaro, O. Tadashi, S. Yasumasa, and O. Shinzaburo, *Chem. Lett.* 1973, **2**, 471-474.

17. (a) T. Schareina, A. Zapf, and M. Beller, *Chem. Commun.* 2004, 1388; (b) A. B. Khemnar, D. N. Sawant, and B. M. Bhanage, *Tetrahedron Lett.* 2013, **54**, 2682-2684; (c) C. W. Liskey, X. Liao, and J. F. Hartwig, *J. Am. Chem. Soc.* 2010, **132**, 11389-11391; (d) A. B. Khemnar, and B. M. Bhanage, *RSC Adv.* 2014, **4**, 13405-13408.

18. (a) M. T. Martin, B. Liu, B. E. Cooley, and J. F. Eaddy, *Tetrahedron Lett.* 2007, **48**, 2555; (b) L. Cai, X. Liu, X. Tao, and D. Shen, *Synth. Commun.* 2004, **34**, 1215; (c) M. Sundermeier, S. Mutyala, A. Zapf, A. Spannenberg, and M. Beller, *J. Organomet. Chem.* 2003, **684**, 50; (d) Y. Ren, Z. Liu, S. Zhao, X. Tian, J. Wang, W. Yin, and S. He, *Catal. Commun.* 2009, **10**, 768; (e) H. Yu, R. N. Richey, W. D. Miller, J. Xu, and S. A. May, *J. Org. Chem.* 2011, **76**, 665.

19. (a) F. H. Luo, C. I. Chu, and C. H. Cheng, *Organometallics* 1998, **17**, 1025; (b) M. Sundermeier, A. Zapf, and M. Beller, *Angew. Chem., Int. Ed.* 2003, **42**, 1661; (c) Z. Zhang, and L. S. Liebeskind, *Org. Lett.* 2006, **8**, 4331; (d) N. Sato, and Q. Yue, *Tetrahedron* 2003, **59**, 5831; (e) P. Anbarasan, H. Neumann, and M. Beller, *Chem. Eur. J.* 2010, **16**, 4725.

20. (a) A. K. Das, S. Nandy, and S. Bhar, *RSC Adv.*, 2022, **12**, 4605-4614; (b) B. N. Patra, A. K. Das, S. Misra, P. P. Jana, P. Brandao, M. Afzal, A. Alarifi, T. Saha, D. Bera, S. Halder, D. Mal, and N. Sepay, *J. Mol. Struct.* 2024, **1300**, 137229; (c) A. K. Das, S. Ali, A. Misra, S. Islam, B. Kar, S. Biswas, G. Ghatak, D. Mal, M. Shit, M. Dolai, and A. Das, *Appl. Organomet. Chem.* 2025, **39**, e7796.

21. (a) P. Yu and B. Morandi, *Angew. Chem., Int.* Ed., 2017, **56**, 15693; (b) Y. Ueda, N. Tsujimoto, T. Yurino, H. Tsurugi, and K. Mashima, *Chem. Sci.*, 2019, **10**, 994-999; (c) F. H. Luo, C. I. Chu and C. H. Chen, *Organometallics*, 1998, **17**, 1025; (d) L. R. Mills, J. M. Graham, P. Patel, and S. A. L. Rousseaux, *J. Am. Chem. Soc.* 2019, **49**, 19257-19262; (e) D. D. Beattie, T. Schareina, and M. Beller, *Org. Biomol. Chem.* 2017, **15**, 4291-4294.

22. (a) A. Sadhukhan, B. N. Patra, T. Maity, A. K. Das, C. K. Ghosh, P. Brandao, D. M. Gil, D. Bera, C. Roy Choudhury, P. K. Bhaumik, D. Mal, and A. Frontera, *Eur. J. Inorg. Chem.* 2024, **27**, e202400459; (b) A. Ghatak, A. Pramanik, A. K. Das and S. Bhar, *Tetrahedron* 2022, **127**, 133090; (c) A. K. Das, S. Saikh, A. Misra, S. Ali, P. Pradhan, N. Sepay, S. Dhibar, M. Afzal, J. Abbas, and N. Sepay, *J. Mol. Struct.* 2026, **1352**, 144012;

View Article Online
DOI: 10.1039/D5MA00879D

(d) A. K. Das, A. Misra, S. Ali, S. Saikh, S. Dhibar, K. K. Banerjee, G. Ghatak, D. Mal, M. Shit, and S. Biswas, *RSC Adv.*, 2025, **15**, 35844-35858.

23. (a) D. Saha, A. K. Das, M. Raish, and N. Sepay, *J. Mol. Struct.* 2025, 1329, 141363; (b) S. Nandy, A. Ghatak, A. K. Das and S. Bhar, *Synlett* 2018, **29**, 2208-2212.
24. A. K. Das, S. Nandy, and S. Bhar, *Appl Organomet Chem.*, 2021, **35**, e6282.
25. Y. Wang, Y. Gao, H. Ding, S. Liu, X. Han, J. Gui, and D. Liu, *Food Chem.* 2017, **218**, 152-158.
26. A. M. Al-Dbass, S. A. Daihan, A. A. Al-Nasser, L. S. Al-Suhaibani, J. Almusallam, B. I. Alnwisser, S. Saloum, R. S. Alotaibi, L. A. Alessa, and R. S. Bhat, *Molecules* 2022, **27**, 7656.
27. P. Adamou, E. Harkou, A. Bumajdad, X. De Jong, M. Van Haute, A. Constantinou, S. M. Al-Salem, *ACS Omega* 2024, **9**, 17, 19057-19062.
28. B. Djebarri, F. Touahra, N. Aider, F. Bali, M. Sehailia, R. Chebout, K. Bachari, and D. Halliche, *Bulletin of Chemical Reaction Engineering & Catalysis* 2020, **15**, 331-347.
29. P. Srimara, T. Chevapruk, P. Kumnorkaew, T. Muangnapoh, P. Vas-Umnuay, Materials Today: *Proceedings,* 2020, **23**, 720-725.
30. A. Bustinza, M. Frías, Y. Liu, and E. García-Bordejé, *Catal. Sci. Technol.* 2020, **10**, 4061-4071.
31. J. Zanon, A. Klapars, and S. L. Buchwald, *J. Am. Chem. Soc.* 2003, **125**, 2890-2891.
32. (a) A. Schareina, A. Zapf, and M. Beller, *J. Organomet. Chem.,* 2004, **689**, 4576-4583; (b) A-R. Hajipour, F. Abrisham, and G. Tavakoli, *Transition Met. Chem.* 2011, **36**, 725-730; (c) B. S. Kumar, A. J. Amali, and K. Pitchumani, *ACS Appl. Mater. Interfaces* 2015, **7**, 22907-22917.
33. (a) M. Binandeh, *J Mater. Sci: Mater Eng.,* 2025, **20**, https://doi.org/10.1186/s40712-025-00212-z; (b) A. Das, D. Chavda, M. Manna, and A. K. Das, *New J. Chem.* 2024, **48**, 18249-18260; (c) A. Das, and A. K. Das, *New J. Chem.* 2023, **47**, 5347-5355; (d) A. K. Das, N. Sepay, S. Nandy, A. Ghatak and S. Bhar, *Tetrahedron Lett.* 2020, **61**, 152231.
34. (a) H. E. Lempers, and R. A. Sheldon, *J. Catal.* 1998, **175**, 62; (b) M. Binandeh, *Nano Trends*, 2025, **11**, 100138.
35. (a) Y. L. Zhang, Z. G. Zhang, Y. Y. Hu, Y. K. Liu, H. W. Jin, and B. W. Zhou*, Org. Biomol. Chem.* 2022, **20**, 8049-8053; (b) Y. J. Wu, C. Ma, M. Bilal, and Y. F. Liang, *Molecules*, 2024, **29**, 6016; (c) Y. Yan, J. Sun, G. Li, L. Yang, W. Zhang, R. Cao, C. Wang, J. Xiao, and D. Xue, *Org. Lett.*, 2022, **24**, 2271-2275; (d) N. A. Wilson, W. M. Palmer, M. K. Slimp, E. M. Simmons, M. V. Joannou, J. Albaneze-Walker, J. M. Ganley,

View Article Online
DOI: 10.1039/D5MA00879D

and D. E. Frantz, *ACS Catal.* 2025, **15**, 6459-6465; (d) F. M. Moghaddam, G. Tavakoli, and H. R. Rezvani, *Appl. Organomet. Chem.* 2014, **28**, 750-755.

36. (a) M. Zamani, A. M. Delfani, and M. Jabbari, *Spectrochimica Acta Part A: Molecular and Biomolecular Spectroscopy* 2018, **201**, 288-299; (b) A. Chahardoli, N. Karimi, X. Ma, and F. Qalekhani, *Scientific Reports* 2020, **10**, 3847.
37. (a) A. Angel Ezhilarasi, J. Judith Vijaya, K. Kaviyarasu, L. John Kennedy, R. Ramalingam, H. A. Al-Lohedan, *J. Photochem. Photobiol. B Biol.* 2018, **180**, 39-50; (b) S. Prabhu, T. D. Thangadurai, P. V. Bharathy, P. Kalugasalam, *Results Chem.* 2022, **4**, 100285; (c) C. R. Rajith Kumar, V. S. Betageri, G. Nagaraj, G. H. Pujar, B. P. Suma, M. S. Latha, *J. Sci. Adv. Mater. Dev.* 2020, **5**, 48-55.
38. (a) K. Ishaq, A. A. Saka, A. O. Kamardeen, A. Ahmed, M. I. H. Alhassan, and H. Abdullahi, *Engineering Science and Technology, an International Journal* 2017, **20**, 563-569; (b) N. A. Amro, L. P. Kotra, K. Wadu-Mesthrige, A. Bulychev, S. Mobashery, and G. Y. Liu, *Langmuir* 2000, **16**, 2789-2796; (c) Y. Hyosuk, D. K. Ji, C. C. Hyun, W. L. Chul, Bull. Korean Chem. Soc. 2013, 34, 3261-3264; (d) M. R. Ahghari, V. Soltaninejad, and A. Maleki, *Scientific Reports* 2020, **10**, 12627.
39. (a) H. El Ghandoor, H. M. Zidan, M. M. Khalil, and M. I. M. Ismail, *Int. J. Electrochem. Sci.* 2012, **7**, 5734-5745; (b) I. M. Obaidat, *Nanomaterials* 2017, **7**, 415; (c) J. Chaudhary, G. Tailor, B. L. Yadav, and O. Michael, *Heliyon* 2019, **5**, 2405-8440; (d) S. B. Park, *Scientific Reports* 2019, **9**, 1-11.
40. (a) S. Mukherjee, S. Dasgupta, S. Sengupta, P. Patra, K. Das, and A. Ghosh, *Langmuir* 2008, **24**, 9817-9826; (b) W. R. Li, X. B. Xie, Q. S. Shi, H. Y. Zeng, O. Y. You-Sheng, and Y.B. Chen, *Applied Microbiology and Biotechnology* 2010, **85**, 1115-1122.
41. (a) B. H. Shnawa, P. J. Jalil, S. M. Hamad, and M. H. Ahmed, *BioNanoSci* 2022, **12**, 1264-1278; (b) Y. Li, P. Leung, L. Yao, Q.W. Song, and E. Newton, *Journal of Hospital Infection* 2006, **1**, 58-63.
42. Y. N. Slavin, J. Asnis, U. O. Häfeli, H. Bach, *J. Nanobiotechnol.* 2017, **15**, 65.

View Article Online
DOI: 10.1039/D5MA00879D

Data Availability Statement

Eco-friendly Cyanation Strategies of Aryl Halides using Recyclable Nickel Nanocatalysts with Promising Antibacterial and Antioxidant Activities

Asit Kumar Das,[a,*] Md Sattar Ali,[a] Arindam Misra,[a] Md Sultan Saikh,[a] Subhendu Dhibar,[b] Sumit Kumar Panja,[c] Aniruddha Das,[d] Gourav Ghatak,[e] Sanjay Bhar,[f] Smritikana Biswas,[e,*]

Data Availability Statement

The data supporting this article have been included as part of the Supplementary Information.